IEEE Access
Multidisciplinary | Rapid Review | Open Access Journal

Received August 27, 2019, accepted October 5, 2019, date of publication October 9, 2019, date of current version October 23, 2019.

Digital Object Identifier 10.1109/ACCESS.2019.2946405

Hybrid Metasurfaces for Infrared-Multiband Radar Stealth-Compatible Materials Applications

CUILIAN XU[1], BINKE WANG[1], YONGQIANG PANG[2], JIAFU WANG[1], MINGBAO YAN[1], WENJIE WANG[1], AIXIA WANG[1], JINMING JIANG[1], AND SHAOBO QU[1]

[1]Department of Basic Science, Air Force Engineering University, Xi'an 710051, China
[2]School of Electronics and Information Engineering, Xi'an Jiaotong University, Xi'an 710049, China

Corresponding authors: Binke Wang (wbk93@163.com) and Shaobo Qu (qushaobo@mail.xjtu.edu.cn)

This work was supported in part by the National Natural Science Foundation of China under Grant 61331005, Grant 61801509, Grant 61771485, Grant 61671467, and Grant 61501502, and in part by the Research Found of Department of Basic Sciences at Air Force Engineering University under Grant JK2019207.

ABSTRACT The compatible stealth functionality in the infrared (IR) and radar wave bands is the most important research topic in the field of stealth material technology. Here, a new hybrid metasurface (HMS) for infrared-multiband radar stealth-compatible materials was proposed and studied. Two specifically designed metasurface layers that can control the infrared emission and microwave absorption were combined to realize radar and IR bi-stealth. The simulated and experimental results show that the HMS has five strong absorption peaks at $f_1 = 6.35$, $f_2 = 8.38$, $f_3 = 12.10$, $f_4 = 15.37$ and $f_5 = 18.05$ GHz. In addition, the emissivity of the proposed HMS is less than 0.32 from 3 to 14 μm and shows low emissivity characteristics in the infrared band. These results demonstrate that the proposal has practical application to multispectral stealth technology.

INDEX TERMS Metasurfaces, infrared-radar stealth-compatible, low emission.

I. INTRODUCTION

Stealth technology is the most important technology for the development of military power under the condition of informational warfare [1]–[5]. The key technology of radar stealth is to reduce the radar echo power or deflect the echo direction, to reduce the radar cross section of the target threat. Infrared (IR) detectors locate, track, guide and attack by detecting the infrared radiation generated by the target. Therefore, the key technology of infrared stealth is to reduce or change the infrared radiation characteristics of the target, which could result in low detection characteristics of the object. Radar-infrared stealth compatibility is the main direction of the stealth materials research field [6]–[8]. In the IR region, the materials require lower emissivity; according to Kirchhoff's law, low emissivity means low absorptivity. However, radar stealth materials require high absorption and low reflection. Obviously, it is very difficult to unify infrared and radar stealth because of their completely opposite working principles. Low-emissivity coatings in the IR wavelength have been used to cover radar stealth materials [9], [10], resulting in worse radar absorption performance. Many efforts have been made to resolve the radar-infrared stealth compatibility in materials science. For example, different types of radar stealth materials have been proposed, such as ordered mesoporous C-MO (M1/4Al, Si, or Ti) nanocomposites [11], [12] or carbon nanotube loaded perovskites with an infrared emissivity of 0.5 [13]. A narrow band microwave absorber of FeAl flake mixtures was fabricated by Lv et al., and the IR emissivity was 0.15 [14]. J.W. Liu demonstrated the crystal structure, electrical conductivity, infrared emissivity and microwave absorption in the La1-xCaxMnO3 system ($0 \leq x \leq 0.5$) [15]. Z.X. Wang proposed a new type of one-dimensional Ge-ZnS photonic crystal with an IR emissivity as low as 0.073 and nearly transparent in terms of radar waves [16]. D. Qi designed a novel composite structure PTFE/Hs/(Ge/ZnS)3 which can realize radarinfraredvisible spectral selective compatibility [17]. For IR wavelengths of 8–14 μm, the proposed structure exhibits an ultralow average

The associate editor coordinating the review of this manuscript and approving it for publication was Weiren Zhu.

emissivity of 0.196 and the average reflectivity is as high as 80.4%. In addition, the proposed structure has an average transmittance of 96.45% in the 2–18 GHz radar wavelength range. When combining these designed structures with radar absorbing materials, radar and IR bi-stealth can also be achieved.

However, in the above scheme, the high microwave absorption and low infrared emission properties are difficult to realize simultaneously and manipulate independently. In recent years, metamaterials that can provide a new way to realize radar-infrared stealth-compatibility have attracted considerable attention for promising applications in the stealth field [18]–[21]. Currently, many techniques have been proposed for realizing metamaterial absorbers [22]–[26]. However, little attention has been paid to their IR stealth properties. Artificial metasurfaces have been proposed to offer a promising new way to manipulate electromagnetic wave radiation [27]–[31]. In addition, the electromagnetic response of metasurfaces has excellent frequency selection characteristics. These metasurfaces are suitable for designing radar and IR bi-stealth structures. For example, H. Tian, and H. F. Cheng designed and fabricated a thin radar and IR bi-stealth structure [7]. C. Zhang and T. J. Cui achieved broadband microwave absorptivity greater than 90% from 8.2 to 16.0 GHz and low infrared emissivity in the IR region of 8–14 μm [32]. Y. Q. Pang and S. B. Qu designed a hybrid metasurface (HMS) that can simultaneously reduce the infrared emission and the microwave reflection [33]. However, few papers have described of the IRSL and RAL design, and multiband tunable radar absorption with low emissivity has not been reported.

In this paper, a new HMS is designed to simultaneously achieve multiband microwave absorption and low IR emission. The frequency peak of the absorption can be easily adjusted by adjusting the length of the resonator. The HMS is composed of a multiband radar absorber layer (RAL) and an infrared shielding layer (IRSL). The low IR emissivity can be flexibly obtained by adjusting the filling ratio (metal area/total area) of the metal part at the top layer. Multiband absorption at microwave frequencies is achieved by designing the geometric parameters of the structural units and thicknesses of the dielectric. In the measurement, the designed HMS exhibits a strong absorptivity over 95% at 6.35, 8.38, 12.10, 15.37 and 18.05 GHz under normal incidence. The experimental results are in good agreement with the simulation. In addition, the emissivity of the proposed HMS is less than 0.32 in the IR band of 3–14 μm. These results are very significant for radar-infrared stealth- compatibility applications.

II. STRUCTURE DESIGN

A. IRSL DESIGN

To achieve infrared-multiband radar stealth-compatibility the development of coating materials with low infrared emissivity is a major problem. The infrared stealth layer satisfies the target low emissivity requirement and allows the radar wave to penetrate the IRSL smoothly such that the radar wave enters the radar stealth layer and is effectively absorbed. An effective way to achieve infrared stealth is to reduce infrared radiation. Consequently, continuous metals are ideal materials for IR stealth, such as aluminum, silver, gold, and copper. However, a continuous metal sheet with a thickness larger than the skin depth will strongly reflect the radar wave. Therefore, a continuous metal sheet is incompatible with radar stealth applications. When the continuous metal sheet is patterned into square patch arrays, electromagnetic waves in the microwave band could transmit through them.

Here, the IRSL is carried out by using a capacitive frequency selective surface (FSS), which has low-pass filtering characteristics. The low IR emissivity could be obtained through a high-filling-ratio metallic material of the FSS. Specifically, the emissivity ε can be calculated as [34]

$$\varepsilon = \varepsilon_m f_m + \varepsilon_d(1 - f_m), \tag{1}$$

where ε is the emissivity of the IRSL, the ε_m and ε_d are the emissivities of the gold metal and dielectric board, respectively. f_m is the filling ratio (metal area/total area) of the metal part. By properly designing the FSS pattern, a low IR emissivity could be realized. Thus, a periodic square copper (Cu) patch structure unit with a high filling ratio was used to achieve high reflection of IR waves. Low-loss material F4B was selected as the dielectric spacer with a dielectric constant of 2.2 and loss tangent of 0.001. The emissivity of Cu is less than 0.1, and the emissivity of the dielectric F4B is less than 0.9 [33]. The gap width between the square patches in the IRSL is $g = 0.1$ mm. This is subject to process precision. Obviously, the larger the copper filling ratio is, the lower the IR emissivity. However, both high microwave transmissivity and low IR emissivity should be consideredsimultaneously when optimizing the structural parameter of the patch width.

The periodic patch metasurface generates ideal reflection characteristics only at the resonant frequency. Radar waves with a frequency lower than the resonant frequency can be transmitted. According to standing wave resonance theory, the resonance frequency can be estimated according to the following equation [35]:

$$f = c/2nw, \tag{2}$$

where w is the width of the Cu patch, $n = \sqrt{\varepsilon_r} = \sqrt{2.2}$ is the refractive index of F4B, and $c = 3 \times 10^8$m/s is the speed of light in a vacuum. Therefore, the smaller the patch size is, the larger the corresponding resonant frequency.

Fig. 1 presents the top view of the IRSL unit cell, which consists of a Cu patch array; the width of the gap is g, and the width of the metallic patch is w. The thickness of F4B is 0.254 mm. The scattering parameters are calculated by the commercial software CST Microwave Studio. The unit cell boundary conditions are set in the x-y plane, and the open boundary condition is chosen to be in the z direction. In the simulations and experiments, the electric conductivity of Cu is 5.8×10^7S/m. Fig.2(a) calculates the microwave

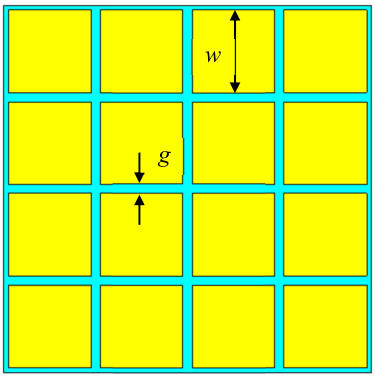

FIGURE 1. Top view of the IRSL structure (yellow indicates metallic copper and blue indicates the F4B board dielectric material).

transmissivity of the IRSL under different patch widths. It can clearly be seen that the smaller the patch size is, the higher the transmissivity of the microwaves in the frequency range from 0 to 20 GHz, especially at high frequencies. When the patch size is 0.9 mm, the transmissivity is 0.88 at 20 GHz, and when the size of the patch is increased to 3 mm, the transmissivity decreases to 0.4 rapidly at 20 GHz. The Cu patch width $w = 0.9$ is determined by theoretical analysis and simulation optimization. According to equation (1), the estimated infrared emissivity is approximately 0.252.

To investigate the stability of wide-angle transmission, the transmissivity under different incident angles from 0° to 60° for TE polarized incident waves is calculated in Fig. 2(b). The corresponding structural parameters are $w = 0.9$ mm and $g = 0.1$ mm. It is observed that, as the angle increases, the transmission at high frequencies is significantly decreased. When the incident angle is 60°, the transmissivity drops to 0.74 at 20 GHz. Fig. 2(c) shows the phase shift in this band. It can clearly be seen that the patch size increased from 0.9 mm to 3.0 mm, and that the corresponding phase shift increased from 26° to 41°. There is a slight difference in the phase shift between these four dimensions.

B. RAL DESIGN

As a subwavelength artificial periodic structure, the absorbing metamaterial can achieve strong absorption of electromagnetic waves if the structure and arrangement of the constituent elements are properly designed. Compared with traditional absorbing materials, metamaterials have the characteristics of perfect absorption, small thickness, light weight and intelligently adjustable. For conventional absorbing metamaterials composed of a metal resonant unit, a lossy medium, and a metal backing plate, the absorbing mechanism can usually be explained by electromagnetic resonance theory. In recent years, with the deepening of absorbing metamaterial research, researchers have proposed a variety of new absorbing mechanisms based on different perspectives: multiple interference theory, standing wave resonance theory, and equivalent circuit theory. These theories play an

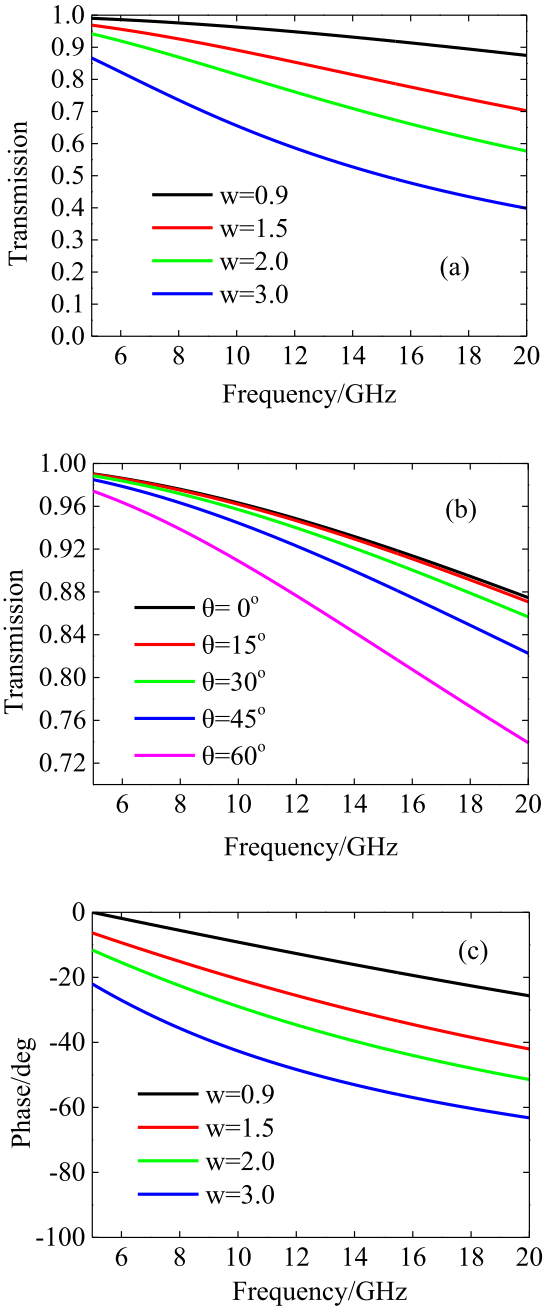

FIGURE 2. (a) The simulated transmissivity under different patch widths; (b) the simulated transmissivity under different incident angles; (c) the simulated phase shift of the IRSL under different patch widths.

important role in the structural design and absorption performance prediction of absorbing metamaterials, especially standing wave resonance theory [35], which can establish the quantitative relationship between the structural and absorption performance of metamaterials. In fact, standing wave resonance theory is the basis for selecting the dimensions of the resonator to resonate at the designated frequency, and it is also the beginning of our design. A metamaterial absorber with two metallic layers can be treated as a planar waveguide, and the fundamental standing wave mode may be estimated

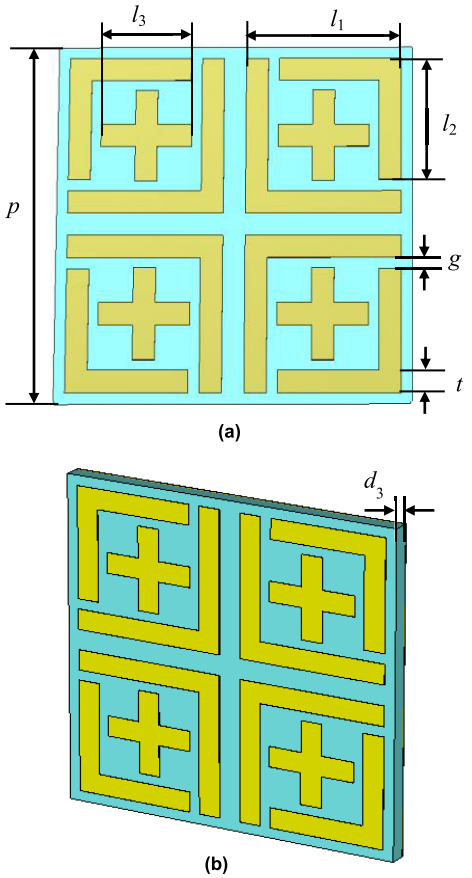

FIGURE 3. The (a) top view and (b) side view of the proposed RAL. (yellow indicates metallic copper, and blue indicates the dielectric material FR4).

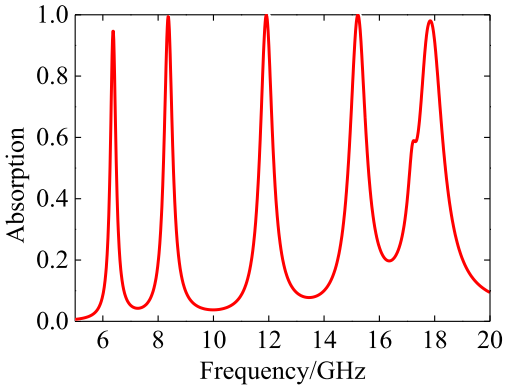

FIGURE 4. Simulated absorption of the RAL under normal incidence.

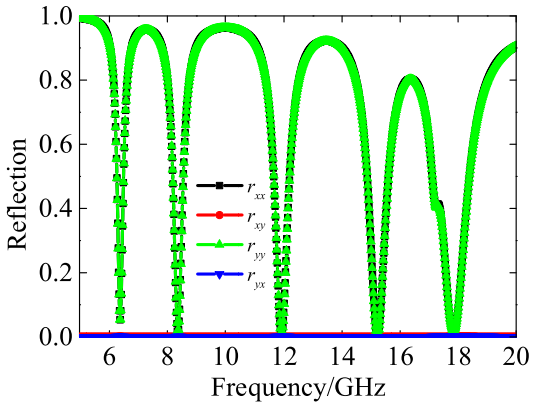

FIGURE 5. Simulated reflections of the co- and cross-polarization under normal incidence.

according to the following equation:

$$f = c/2nL, \tag{3}$$

where L is the length of the resonator $n = \sqrt{\varepsilon_r} = \sqrt{4.3}$ is the refractive index of FR4, and $c = 3 \times 10^8$m/s is the speed of light in a vacuum.

Fig.3 shows the designed RAL structure, which consists of three layers: four groups of metallic L-shaped resonators and cross resonators located at the front and a metallic plane at the back, separated by a dielectric layer. The high-loss FR4 material was selected as the dielectric spacer, with a dielectric constant of 4.3 and loss tangent of 0.025 in the RAL layer. The thickness of FR4 is $d_3 = 0.8$ mm. The corresponding structural parameters are $l_1 = 7.0$ mm, $l_2 = 5.5$ mm, $l_3 = 4.0$ mm, $t = 1.0$ mm, $g = 0.5$ mm, and $p = 16$mm. Inserting the length $L = 2(l_1\text{-}t) = 12$ mm into equation (3), we obtain $f = 6.03$ GHz which is basically in accordance with that of the simulation result $f = 6.35$ GHz, as illustrated in Fig.4. The RAL has the same electromagnetic response to TE and TM polarizations because the design has a fourfold rotational symmetry; thus, Fig.4 shows only the electromagnetic response of the TE mode. It can be seen that the proposed RAL has five distinctive absorption peaks at $f_1 = 6.35$, $f_2 = 8.38$, $f_3 = 11.93$, $f_4 = 15.25$ and $f_5 = 17.86$ GHz under normal incidence, with absorbances of 94.6%, 99.2%, 99.2%, 99.6% and 98.0%, respectively. Moreover, because the structure seems to be chiral resulting in TE-TM conversion, the microwave reflections of the co- and cross-polarization were rechecked carefully. The co- and cross-polarization were defined as $r_{xx} = |E_{xr}/E_i|$ and $r_{xy} = |E_{yr}/E_i|$ for x-polarized incidence, respectively. As shown in Fig.5, due to the fourfold rotational symmetry of the structure, the cross-polarization reflections r_{xy} and r_{yx} both approached 0 at 0–20 GHz.

C. DESIGN OF IR-RADAR BI-STEALTH STRUCTURE

Based on the preceding analysis in sections A and B, due to the completely opposite stealth principles in the microwave and IR wavelength bands, the HMS is composed of two different-sized copper structures. The designed IRSL and RAL are combined to achieve IR and radar bi-stealth. As shown in Fig. 6 (a), the designed HMS has five layers, a metal/dielectric /metal/dielectric/metal construction. The low-loss F4B material was selected as the dielectric spacer, with a dielectric constant of 2.2 and loss tangent of 0.001 in the IRSL layer. The thickness of F4B is $d_1 = 0.254$ mm. The high-loss FR4 material was selected as the dielectric spacer, with a dielectric constant of 4.3 and loss tangent of

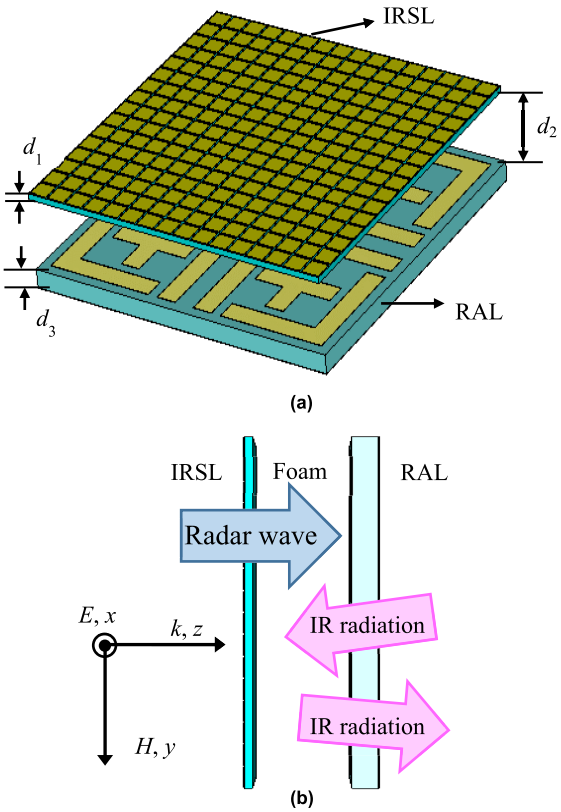

FIGURE 6. The proposed structure of the HMS. (a) Perspective view of the HMS; (b) side view of the HMS (yellow indicates metallic copper and blue indicates the dielectric material).

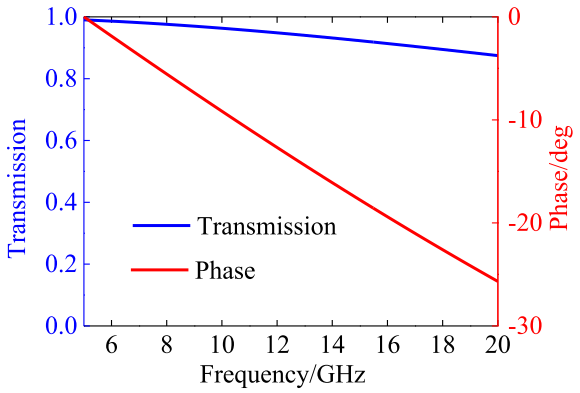

FIGURE 7. The simulated transmissivity and phase shift of the IRSL.

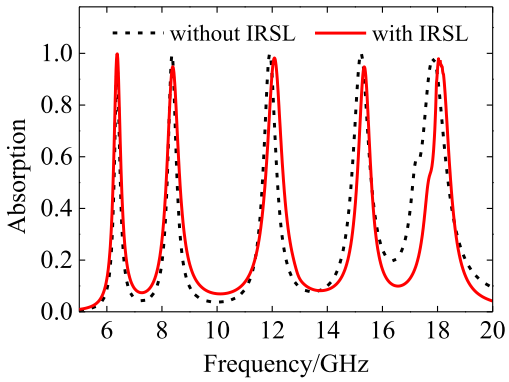

FIGURE 8. Simulated absorption of the HMS under normal incidence with and without the IRSL.

0.025 in the RAL layer. The thickness of FR4 is $d_3 = 0.8$ mm. The RAL is separated from the IRSL by a foam board at a distance $d_2 = 3.0$ mm. The dielectric constant of foam is 1.03. The gap width of the IRSL is 0.1 mm, and the width of the copper (Cu) patch is 0.9 mm. The incident wave can efficiently pass through the top copper array because the microwave wavelength of interest is much larger than the size of the square patches. The RAL electromagnetic resonators consisted of four groups of L-shaped resonators and cross resonators, as shown in Fig. 3. The corresponding parameters are $l_1 = 7.0$ mm, $l_2 = 5.5$ mm, $l_3 = 4.0$ mm, $t = 1.0$ mm, $g = 0.5$ mm and $p = 16$ mm. The unit cell has periodic dimensions of 16 mm, and there are 16×16 subcells in the IRSL and a 1×1 sub-cell in the RAL in one repeated period.

III. RESULTS AND DISCUSSION

To reveal the effect of the IRSL on the microwave performance, the transmissivity and phase of the IRSL are calculated under normal incidence in Fig.7. When patterned into square patch arrays, the IRSL becomes nearly transparent to microwaves below 20 GHz. The transmissivity is larger than 88%, and the phase shift in this band is 26°. The metal square patches have a very weak dipolar interaction with the incident wave at frequencies from 0 to 20 GHz because of the large operating wavelength compared with the element size, and the square patch arrays compose a thin dielectric surface that perturbs the incident wave slightly. The IRSL has high-efficiency transmission for microwaves below 20 GHz which is below its resonant frequency. The resonant frequency can be changed by controlling the size of the square patch and the gap of the component and to achieve frequency selective absorption and transmission. The high reflectivity of the IRSL mainly depends on the filling ratio of the metal. Therefore, a high filling ratio is required to achieve high reflection and low emission for the infrared stealth function.

Fig. 8 shows the absorption of the HMS under normal incidence for the TE mode. It can be seen that the proposed HMS has five distinctive absorption peaks at $f_1 = 6.35$, $f_2 = 8.38, f_3 = 12.10, f_4 = 15.37$ and $f_5 = 18.05$ GHz under normal incidence, with absorbances of 99.8%, 94.6%, 97.8%, 94.7% and 98.8%, respectively. Compared to the absorption of the structure without the IRSL, it was observed that the absorption peak undergoes a slight change when the IRSL is added. This can be explained by the mutual coupling between the other layers and the IRSL.

To investigate the wide-angle stability, the absorptions are calculated with the incident angle θ varying from 0°to 45° for both TE and TM polarized incident waves. Fig. 9 (a) shows that the absorption is higher than 92.5% at these five resonance frequencies with an incident angle up to 45° for TE polarization. With the incident angle up to 45°,

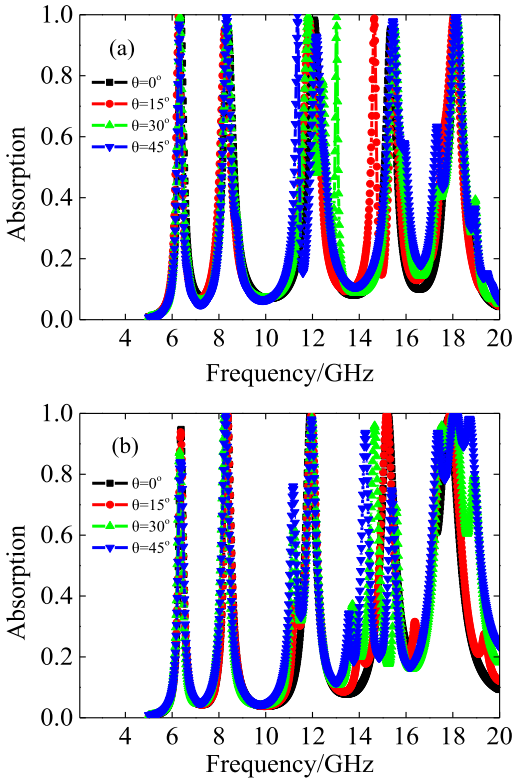

FIGURE 9. Simulated wide-angle absorption under different incident angles up to 45°: (a) TE and (b) TM polarized.

the absorption remains higher than 82.8% at these five resonance frequencies for TM polarization. It should be noted that with increasing incident angle, however, the absorption peaks at 12.10 and 15.37 GHz split into two separate absorption peaks for both TE and TM polarizations. These additional peaks are caused mainly by the parasitic resonances of the proposed structure [36], [37]. Moreover, for TM polarization, the band of absorption at 18.05 GHz becomes wider as the incident angle increased to 45°.

To better understand the absorption behavior of the proposed HMS, we further investigate the distribution of the z-component electric field E_z at the resonant frequencies. Fig.10 gives the distribution of E_z in the plane z = 0.5 mm, which is just the center plane of FR4. It can be clearly observed that strong enhancement of the electric fields is excited at specific positions for the specific frequency. The resonance frequencies are mainly determined by the length of the resonators. Fig. 10 (a) shows that opposite charges accumulate on both sides of the long L-shaped resonator. This is also true for a short L-shaped resonator, as shown in Fig.10 (b). These two resonant modes at frequencies of 6.35 and 8.38 GHz indicate excitation of the dipole resonances in the metallic structure. Fig.10 (c) and Fig. 10 (d) show that the resonant modes at frequencies 12.10 and 15.37 GHz are both quadrupole resonances of the L-shaped resonators. Fig. 10 (e) shows that opposite

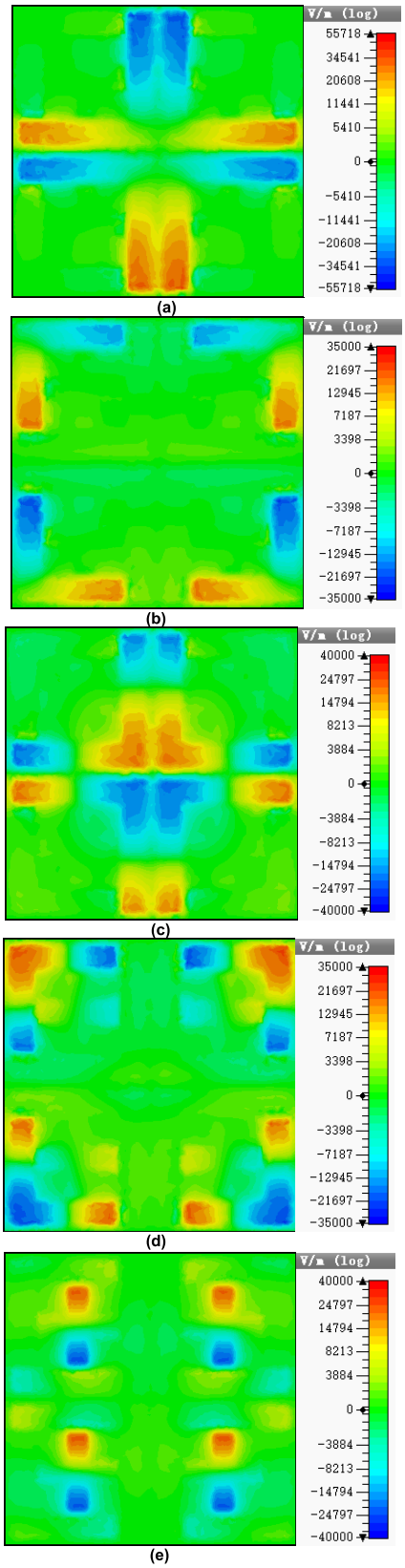

FIGURE 10. Distributions of the z-component electric field E_Z in the plane z = 0.5 mm, which is just the center plane of FR4. (a) f_1 = 6.35 GHz, (b) f_2 = 8.38 GHz, (c) f_3 = 12.10 GHz, (d) f_4 = 15.37 GHz and (e) f_5 = 18.05 GHz.

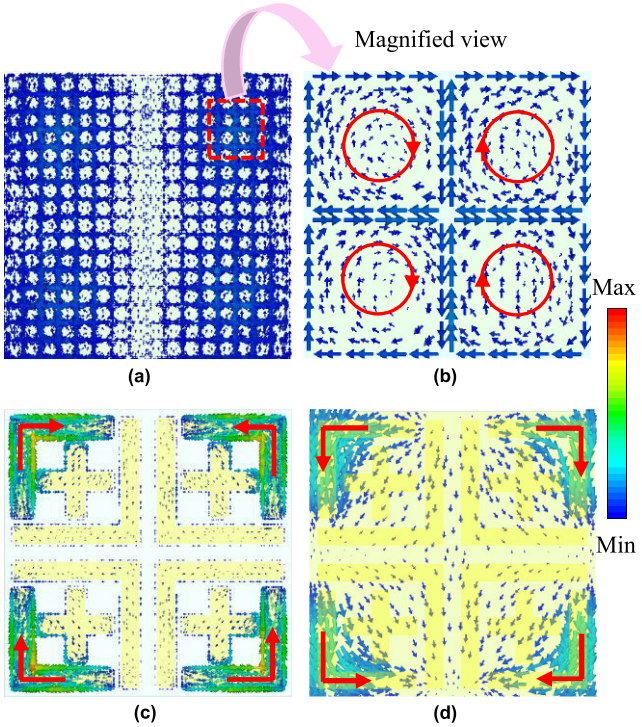

FIGURE 11. Distributions of surface current resonance frequency $f = 8.38$ GHz: (a) the surface currents on the top layer, (b) magnified view of the surface currents on the top layer, (c) the surface currents on the metal resonant unit, and (d) the surface currents on the metal backing plate.

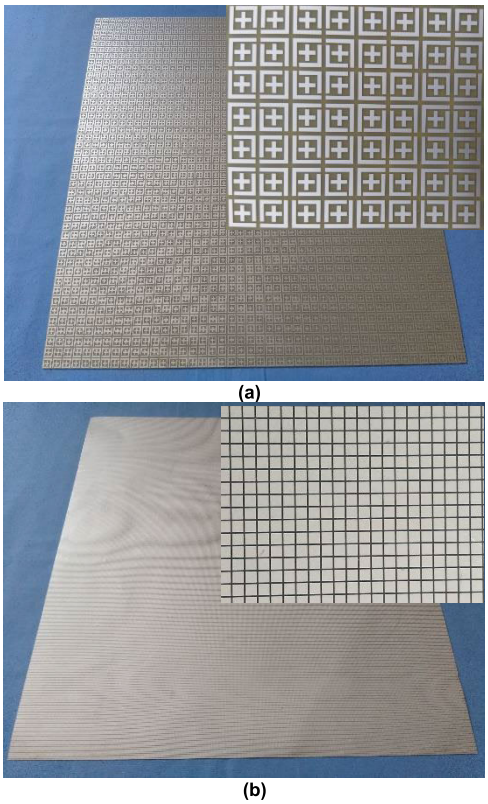

FIGURE 12. Photographs of the fabricated layers: (a) RAL and (b) IRSL. The inserted image is a larger version of the layer.

charges are mainly concentrated on the edges of the four-point cross, demonstrating the excitation of the electric dipole resonance in cross resonators. This results in 97% absorption at 18.05 GHz. Moreover, the resonances for 12.10 and 15.37 GHz correspond to the second-order resonance mode of the short and long L-shaped resonators, respectively.

Fig.11 presents the surface current distributions at the second resonance frequency $f = 8.38$ GHz. As shown in Fig. 11 (a), most of the currents on the top layer are primarily confined to the copper patches, and the closed current loop (Fig.11 (b)) forms magnetic resonance with intense magnetic fields. Fig. 11 (c) shows that at a resonant frequency of 8.38 GHz, the surface currents are mainly concentrated on the short L-shaped resonators while anti-parallel currents are found to exist on the metal backing plate (Fig.11 (d)), indicating the formation of magnetic resonance with intense magnetic fields. Therefore, the high absorption at the resonance frequency of the proposed structure is mainly caused by the magnetic resonance between the metal resonant unit and the metal backing plate of the RAL.

IV. EXPERIMENTAL DEMONSTRATION

To confirm the design and simulation results of the HMS, a 380 mm×380 mm sample was fabricated using the printed circuit board technique. The metal is a copper film and the thickness of the copper is 0.017 mm. The dielectric of the RAL is a high-loss dielectric FR4 board. The periodic radar absorber structure was fabricated on the FR4 board, as shown in Fig. 12 (a). The dielectric of the IRSL is a low-loss dielectric F4B board. Low-emissivity periodic square patch arrays were etched on the F4B boards as shown in Fig. 12 (b). The artificial structure was then obtained by sticking the RAL and IRSL on the sides of the foam board together. The total thickness of our proposed infrared-multiband radar bi-stealth device is 4.108 mm.

The reflection properties of the IR-radar bi-stealth structure samples at microwave frequencies were measured with the free space reflection method in a microwave anechoic chamber. An Agilent 8720ET vector network analyzer was used to measure the reflection. Two horn antennas were connected to the vector network analyzer, and they acted as electromagnetic wave transmitters and receivers, respectively. Real pictures of the measurement location are shown in Fig.13: the incident waves were perpendicular to the sample. The distance from the position of the HMS sample plate to both horn antennas was the same, that is, 507.9 mm. When conducting the measurements, the reflection of a metal plate with the same size as the artificial structure is first measured to normalize. The absorption spectra of the HMS were measured and compared with the simulated result, as shown in Fig. 14. It can be seen that the measured results are consistent with the simulated results, except for a slight shift towards low frequencies. This deviation is mainly due to the

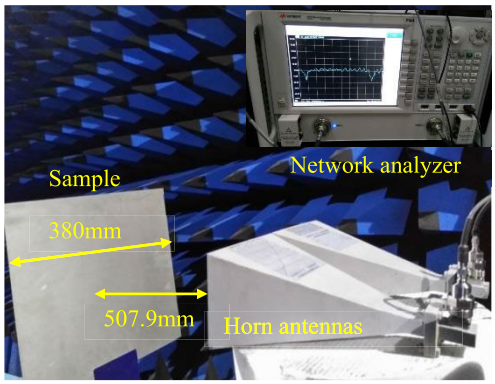

FIGURE 13. Real pictures of the experimental measurement system. The inserted image is an Agilent 8720ET vector network analyzer.

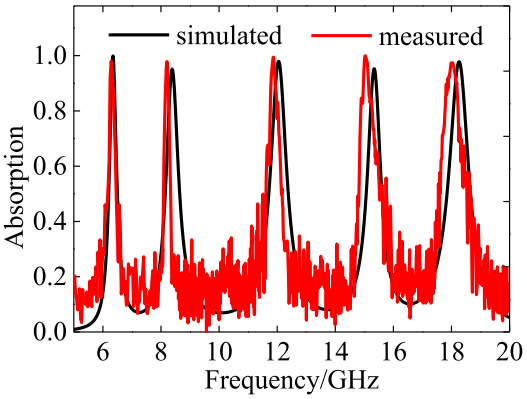

FIGURE 14. Measured and simulated absorption spectra of the HMS structure under normal incidence.

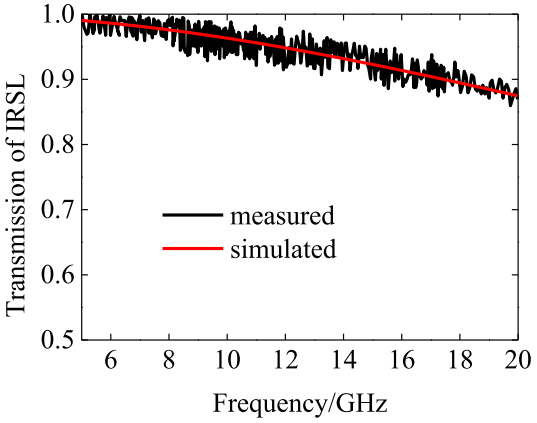

FIGURE 15. Measured and simulated transmission spectra of the IRSL under normal incidence.

dielectric constant difference between the simulated and the actual material parameters. The transmission spectra of the IRSL were measured and are shown in Fig.15. It can be observed that the transmissivity from 0 GHz to 20 GHz is higher than 0.86 and maintains good microwave transparency.

Due to the large difference between the operating wavelength of the electromagnetic waves and the size of the structural units, it is difficult to obtain the simulated emissivity

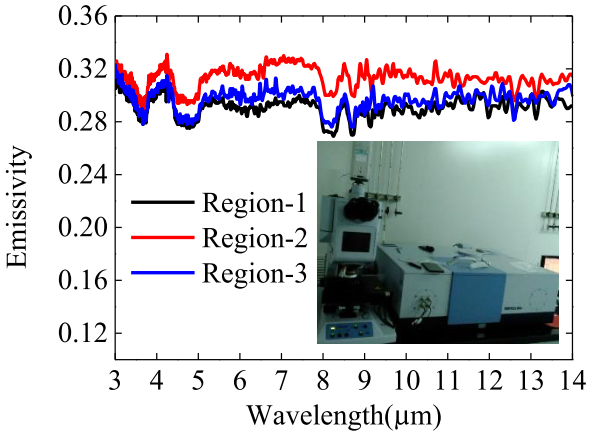

FIGURE 16. Measured emissivity spectra of the fabricated HMS at the infrared band. The inserted image is the measurement setup photo.

of the infrared-multiband radar bi-stealth structure. Therefore, only the experimental discussion results are given here. According to Kirchhoff's law, the emissivity of a material is equal to the absorption rate under equilibrium conditions. Therefore, we can obtain the infrared emissivity by measuring the reflection spectra of the structure. Vertex 80 was used in the measurement of reflection at the 3–14 μm IR band. We select three different regions from the sample to measure. The emissivity of the sample is shown in Fig. 16 which was calculated from the measured reflection rate. It can be seen that over the whole infrared band of 3–14 μm, the emissivities of the three different regions are all less than 0.32, which is close to the value estimated. The emissivity of the IRSL can be kept close to that of the continuous metal film by tailoring the metal filling ratio.

V. CONCLUSION

In conclusion, a new HMS of IR and radar bi-stealth structures has been designed and fabricated to achieve multiband microwave absorption and infrared stealth simultaneously. The HMS is constructed by stacking a multiband radar absorber and an infrared shielding structure. The thickness of the HMS is 4.108 mm. Both simulated and experimental results indicate that the HMS has five strong absorption peaks at 6.35, 8.38, 12.10, 15.37 and 18.05 GHz. The electric field E_z and surface currents at the resonant frequencies were discussed to reveal the electromagnetic mechanism of absorption. Moreover, the emissivity of the structure is as low as 0.32 in the 3–14μm IR band, which satisfies the requirements of infrared stealth technology. In general, the HMS of the radar and IR bi-stealth structures, which shows promising potential applications for multifunctional stealth technology, is confirmed both numerically and experimentally.

REFERENCES

[1] G. A. Rao and S. P. Mahulikar, "Integrated review of stealth technology and its role in airpower," *Aeronaut. J.*, vol. 106, no. 1066, pp. 629–642, Dec. 2002.

[2] D. Qi, X. Wang, Y. Cheng, R. Gong, and B. Li, "Design and characterization of one-dimensional photonic crystals based on ZnS/Ge for infrared-visible compatible stealth applications," *Opt. Mater.*, vol. 62, pp. 52–56, Dec. 2016.
[3] M. L. Immordino, F. Dosio, and L. Cattel, "Stealth liposomes: Review of the basic science, rationale, and clinical applications, existing and potential," *Int. J. Nanomed.*, vol. 1, no. 3, pp. 297–315, Sep. 2006.
[4] Y. Pang, Y. Shen, Y. Li, J. Wang, Z. Xu, and S. Qu, "Water-based metamaterial absorbers for optical transparency and broadband microwave absorption," *J. Appl. Phys.*, vol. 123, no. 15, 2018, Art. no. 155106.
[5] J. Kim, K. Han, and J. W. Hahn, "Selective dual-band metamaterial perfect absorber for infrared stealth technology," *Sci. Rep.*, vol. 7, Jul. 2017, Art. no. 6740.
[6] M. S. Kluskens and E. H. Newman, "Scattering by a chiral cylinder of arbitrary cross section," *IEEE Trans. Antennas Propag.*, vol. 38, no. 9, pp. 1448–1455, Sep. 1990.
[7] H. Tian, L. Hai-Tao, and C. Hai-Feng, "A thin radar-infrared stealth-compatible structure: Design, fabrication, and characterization," *Chin. Phys. B*, vol. 23, no. 2, 2014, Art. no. 025201.
[8] S. Zhong, L. Wu, T. Liu, J. Huang, W. Jiang, and Y. Ma, "Transparent transmission-selective radar-infrared bi-stealth structure," *Opt. Express*, vol. 26, no. 13, pp. 16466–16476, Jun. 2018.
[9] L. Liu, R. Gong, Y. Cheng, F. Zhang, H. He, and D. Huang, "Emittance of a radar absorber coated with an infrared layer in the 3-5μm window," *Opt. Express*, vol. 13, no. 25, pp. 10382–10391, 2005.
[10] S. Fantucci and V. Serra, "Investigating the performance of reflective insulation and low emissivity paints for the energy retrofit of roof attics," *Energy Buildings*, vol. 182, pp. 300–310, Jan. 2019.
[11] T. Wang, J. He, J. Zhou, X. Ding, J. Zhao, S. Wu, and Y. Guo, "Electromagnetic wave absorption and infrared camouflage of ordered mesoporous carbon–alumina nanocomposites," *Microporous Mesoporous Mater.*, vol. 134, no. 3, pp. 58–64, 2010.
[12] J. Zhou, J. He, G. Li, T. Wang, D. Sun, X. Ding, J. Zhao, and S. Wu, "Direct incorporation of magnetic constituents within ordered mesoporous carbon-silica nanocomposites for highly efficient electromagnetic wave absorbers," *J. Phys. Chem. C*, vol. 114, no. 17, pp. 7611–7617, 2010.
[13] L. Chen, C. Lu, Z. Fang, Y. Lu, Y. Ni, and Z. Xu, "Infrared emissivity and microwave absorption property of $Sm_{0.5}Sr_{0.5}CoO_3$ perovskites decorated with carbon nanotubes," *Mater. Lett.*, vol. 93, pp. 308–311, Feb. 2013.
[14] H. Lv, G. Ji, X. Li, X. Chang, M. Wang, H. Zhang, and D. Youwei, "Microwave absorbing properties and enhanced infrared reflectance of FeAl mixture synthesized by two-step ball-milling method," *J. Magn. Magn. Mater.*, vol. 374, pp. 225–229, Jan. 2015.
[15] J. W. Liu, J. J. Wang, and H. T. Gao, "Infrared emissivities and microwave absorption properties of perovskite $La_{1-x}Ca_xMnO_3$ ($0 \leq x \leq 0.5$)," *Mater. Sci. Forum*, vol. 914, pp. 96–101, Feb. 2018.
[16] Z. Wang, Y. Cheng, Y. Nie, X. Wang, and R. Gong, "Design and realization of one-dimensional double hetero-structure photonic crystals for infrared-radar stealth-compatible materials applications," *J. Appl. Phys.*, vol. 116, no. 5, 2014, Art. no. 054905.
[17] D. Qi, Y. Cheng, X. Wang, F. Wang, B. Li, and R. Gong, "Multi-layer composite structure covered polytetrafluoroethylene for visible-infrared-radar spectral compatibility," *J. Phys. D, Appl. Phys.*, vol. 50, no. 50, 2017, Art. no. 505108.
[18] X. Shen, T. J. Cui, J. Zhao, H. F. Ma, W. X. Jiang, and H. Li, "Polarization-independent wide-angle triple-band metamaterial absorber," *Opt. Express*, vol. 19, no. 10, pp. 9401–9407, 2011.
[19] J. Zhao, Q. Cheng, J. Chen, M. Q. Qi, W. X. Jiang, and T. J. Cui, "A tunable metamaterial absorber using varactor diodes," *New J. Phys.*, vol. 15, Apr. 2013, Art. no. 043049.
[20] F. Ding, Y. Cui, X. Ge, Y. Jin, and S. He, "Ultra-broadband microwave metamaterial absorber," *Appl. Phys. Lett*, vol. 100, no. 10, 2012, Art. no. 103506.
[21] C. Zhang, Q. Cheng, J. Yang, J. Zhao, and T. J. Cui, "Broadband metamaterial for optical transparency and microwave absorption," *Appl. Phys. Lett.*, vol. 110, no. 14, 2017, Art. no. 143511.
[22] M. Pu, C. Hu, M. Wang, C. Huang, Z. Zhao, C. Wang, Q. Feng, and X. Luo, "Design principles for infrared wide-angle perfect absorber based on plasmonic structure," *Opt. Express*, vol. 19, no. 18, pp. 17413–17420, Aug. 2011.
[23] L. Huang, D. R. Chowdhury, S. Ramani, M. T. Reiten, S. N. Luo, A. J. Taylor, and H. T. Chen, "Experimental demonstration of terahertz metamaterial absorbers with a broad and flat high absorption band," *Opt. Lett.*, vol. 37, no. 2, pp. 154–156, 2012.
[24] Y. Cui, K. H. Fung, J. Xu, H. Ma, Y. Jin, S. He, and N. X. Fang, "Ultra-broadband light absorption by a sawtooth anisotropic metamaterial slab," *Nano Lett.*, vol. 12, no. 3, pp. 1443–1447, 2012.
[25] W. J. Wang, J. Wang, M. Yan, J. Wang, H. Ma, M. Feng, and S. Qu, "Dual band tunable metamaterial absorber based on cuboid ferrite particles," *J. Phys. D, Appl. Phys.*, vol. 51, no. 31, 2018, Art. no. 315001.
[26] J. Ma, Z. Ma, W. Sun, F. Ding, Q. He, L. Zhou, and Y. Ma, "Ultra-broadband terahertz metamaterial absorber," *Appl. Phys. Lett.*, vol. 105, no. 2, Jul. 2014, Art. no. 021102.
[27] N. Yu, P. Genevet, M. A. Kats, F. Aieta, J.-P. Tetienne, F. Capasso, and Z. Gaburro, "Light propagation with phase discontinuities: Generalized laws of reflection and refraction," *Science*, vol. 334, no. 6054 , pp. 333–337, 2011.
[28] S. Sun, Q. He, S. Xiao, Q. Xu, X. Li, and L. Zhou, "Gradient-index metasurfaces as a bridge linking propagating waves and surface waves," *Nature Mater.*, vol. 11, no. 5, pp. 426–431, 2012.
[29] L. Huang, X. Chen, H. Mühlenbernd, G. Li, B. Bai, Q. Tan, G. Jin, T. Zentgraf, and S. Zhang, "Dispersionless phase discontinuities for controlling light propagation," *Nano Lett.*, vol. 12, no. 11, pp. 5750–5755, 2012.
[30] A. Pors and S. I. Bozhevolnyi, "Plasmonic metasurfaces for efficient phase control in reflection," *Opt. Express*, vol. 21, no. 22, pp. 27438–27451, Nov. 2013.
[31] C. Pfeiffer and A. Grbic, "Metamaterial Huygens' surfaces: Tailoring wave fronts with reflectionless sheets," *Phys. Rev. Lett.*, vol. 110, no. 19, May 2013, Art. no. 197401.
[32] C. Zhang, J. Yang, W. Yuan, J. Zhao, J. Y. Dai, T. C. Guo, J. Liang, G. Y. Xu, Q. Cheng, and T. J. Cui, "An ultralight and thin metasurface for radar-infrared bi-stealth applications," *J. Phys. D, Appl. Phys.*, vol. 50, no. 44, 2017, Art. no. 444002.
[33] Y. Pang, Y. Li, M. Yan, D. Liu, J. Wang, Z. Xu, and S. Qu, "Hybrid metasurfaces for microwave reflection and infrared emission reduction," *Opt. Express*, vol. 26, no. 9, pp. 11950–11958, 2018.
[34] S. Zhong, W. Jiang, P. Xu, T. Liu, J. Huang, and Y. Ma, "A radar-infrared bi-stealth structure based on metasurfaces," *Appl. Phys. Lett.*, vol. 110, no. 6, 2017, Art. no. 063502.
[35] X.-Y. Peng, B. Wang, S. Lai, D. H. Zhang, and J.-H. Teng, "Ultrathin multi-band planar metamaterial absorber based on standing wave resonances," *Opt. Express*, vol. 20, no. 25, pp. 27756–27765, Nov. 2012.
[36] S. Shang, S. Yang, L. Tao, L. Yang, and H. Cao, "Ultrathin triple-band polarization-insensitive wide-angle compact metamaterial absorber," *AIP Adv.*, vol. 6, no. 7, 2016, Art. no. 075203.
[37] H.-X. Xu, G.-M. Wang, M.-Q. Qi, J.-G. Liang, J.-Q. Gong, and Z.-M. Xu, "Triple-band polarization-insensitive wide-angle ultra-miniature metamaterial transmission line absorber," *Phys. Rev. B, Condens. Matter*, vol. 86, no. 20, Nov. 2012, Art. no. 205104.

CUILIAN XU received the B.S. degree in physics from Liaocheng University, Liaocheng, China, in 2006, and the M.S. degree in optics from the Harbin Institute of Technology, Harbin, China, in 2008. Since 2008, she has been employed with Air Force Engineering University, Xi'an, where she is currently an Associate Professor in physical electronics. Her current research interests include design of metamaterials and application of the metamaterials.

BINKE WANG received the B.S. degree in physics from the National University of Defense Technology, Changsha, Hunan, China, in 1984, the M.S. degree in physical electronics from Air Force Engineering University, Xi'an, Shaanxi, China, in 1999, where he is currently a Professor in physical electronics. His research interest includes the infrared stealth materials and technology.

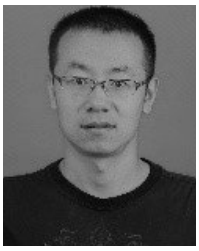

YONGQIANG PANG received the B.S. degree from the University of Electronic Science and Technology of China, Chengdu, China, in 2007, the M.S. and Ph.D. degrees from the National University of Defense Technology, Changsha, in 2010 and 2013, respectively. He is currently an Associate Professor with the School of Electronic Science and Engineering, Xi'an Jiaotong University, Xi'an, China. His research interests include frequency selective surfaces, metamaterials, and electromagnetic composite materials.

JIAFU WANG received the B.S. degree in radar engineering, the M.S. degree in optics engineering, and the Ph.D. degree in physical electronics from Air Force Engineering University, Xi'an, Shaanxi, China, in 2004, 2007, and 2010, respectively. He is currently an Associate Professor in physical electronics. His current research interests include mainly on plasma stealth, design of metamaterials, and application of the metamaterials in microwave devices.

MINGBAO YAN received the B.S. and M.S. degrees in physics from Qufu Normal University, Qufu, China, in 2005 and 2008, respectively, and the Ph.D. degree in physical electronics from Air Force Engineering University, Xi'an, Shaanxi, China, in 2016. Since 2008, he has been with Air Force Engineering University, where he is currently an Associate Professor in physical electronics. His current research interests include frequency selective surface and the design of stealth radome metamaterial.

WENJIE WANG received the B.S. degree in physics from Ludong University, Yantai, China, in 2005, and the M.S. degree in optics from the Beijing Institute of Technology, Beijing, China, in 2008. Since 2008, she has been with Air Force Engineering University, where she is currently a Lecturer in physics. Her current research interests include in all medium metamaterial and the design of stealth radome metamaterial.

AIXIA WANG received the B.S. and M.S. degrees in physics from Shaanxi Normal University, Xi'an, Shaanxi, China, in 2003 and 2006. Since 2006, she has been employed with Air Force Engineering University, Xi'an, where she is currently an Associate Professor in physical electronics. Her current research interests include design of metamaterials and application of the metamaterials.

JINMING JIANG received the B.S. degree in materials from Sichuan University, Chengdu, Sichuan, China, in 2010, and the M.S. and Ph.D. degrees in materials from the National University of Defense and Technology, Changsha, Hunan, China, in 2013 and 2017, respectively. He has been employed with Air force Engineering University, since 2017. His scientific interests include the design and fabrication of micro/nanao and composite materials. His current research interests include the characteristic of metamaterials and integrated manufacturing of composite structure.

SHAOBO QU received the B.S. degree in physics from Fuyang Normal College, Fuyang, Anhui, China, in 1984, the M.S. degree in physics from Sichuan Normal University, Chengdu, China, in 1991, and the Ph.D. degree in materials science and engineering from Northwest Polytechnical University, Xi'an, China, in 2001. Since 2001, he has been with the Department of Applied Mathematics and Physics, Air Force Engineering University, Xi'an, China, where he is currently a Professor in physical electronics. His research interests include materials physics, metamaterials, and electronic materials and devices.